J Mol Model (2012) 18:3255–3266
DOI 10.1007/s00894-011-1342-7

ORIGINAL PAPER

Quantum-mechanical computations on the electronic structure of *trans*-resveratrol and *trans*-piceatannol: a theoretical study of the stacking interactions in *trans*-resveratrol dimers

Damian Mikulski · Marcin Molski

Received: 29 July 2011 / Accepted: 19 December 2011 / Published online: 15 January 2012

Abstract Accurate quantum-chemical calculations based on the second-order Møller–Plesset perturbation method (MP2) and density functional theory (DFT) were performed for the first time to investigate the electronic structures of *trans*-resveratrol and *trans*-piceatannol, as well as to study the stacking interaction between *trans*-resveratrol molecules. Ab initio MP2 calculations performed with using standard split-valence Pople basis sets led us to conclude that these compounds have structures that deviate strongly from planarity, whereas the DFT computations for the same basis sets revealed that the equilibrium geometries of these bioactive polyphenols are planar. Furthermore, the results obtained at the MP2(full)/aug-cc-pVTZ and B3LYP/aug-cc-pVTZ levels indicated that the geometries of *trans*-resveratrol and *trans*-piceatannol are practically planar at their absolute energy minima. The relative energies of the equilibrium geometries of *trans*-resveratrol on its potential energy surface were computed at the MP2(full)/aug-cc-pVTZ level. According to the results obtained, a T-shaped (edge-to-phase) conformer of *trans*-resveratrol dimer is the most stable in vacuum. This T-shaped conformer is mainly stabilized by strong hydrogen bonding and weak C–H…π interactions. Stacked structures with parallel-displaced *trans*-stilbene skeletons were also found to be energetically stable. The vertical separation and twist angle dependencies of the stacking energy were investigated at the MP2(full)/aug-cc-pVTZ, B3LYP/aug-cc-pVTZ, and HF/aug-cc-pVTZ levels. The standard B3LYP functional and the Hartree–Fock method neglect long-range attractive dispersion interactions. The MP2 computations revealed that the London dispersion energy cannot be neglected at long or short distances. The stacked model considered here may be useful for predicting the quantum nature of the interactions in π-stacked systems of other naturally occurring stilbenoids, and can help to enhance our understanding of the antioxidant and anticancer activities of *trans*-resveratrol.

Keywords *Trans*-resveratrol · *Trans*-piceatannol · MP2 method · Ab initio study · DFT method · Stacking interaction

D. Mikulski (✉) · M. Molski
Department of Theoretical Chemistry, Faculty of Chemistry,
A. Mickiewicz University ul,
Grunwaldzka 6,
60-780 Poznań, Poland
e-mail: dmkwant@amu.edu.pl

Introduction

Due to the existence of the French Paradox (i.e., that French people have a surprisingly low incidence of coronary heart disease considering that their diets tend to be rich in saturated fats), polyphenolic derivatives of *trans*-stilbene—such as *trans*-resveratrol (*trans*-3,4′,5-trihydroxystilbene, *t*-RES) and *trans*-piceatannol (*trans*-3′,4′,3,5-tetrahydroxystilbene, *t*-PIC)—have been studied with great intensity by many scientists, from chemists to medical researchers. These compounds are common phytoalexins that act as toxins to the attacking pathogens of plants. They can be found in fruit and vegetables, which are important dietary components. Over the past twenty years, many experimental studies have provided interesting insights into the ground-state geometries of *t*-RES and *t*-PIC.

Trans-resveratrol (Fig.1a) can be found mainly in grapes, mulberries, and peanuts [1, 2]. The bioactivity of *t*-RES has been widely investigated. This compound is a significant antioxidant, anticarcinogenic, and anti-inflammatory agent [1]. The structural features of this compound were studied by X-ray diffraction and reported by Caruso et al. [3]. The results obtained indicated that at room temperature, *t*-RES

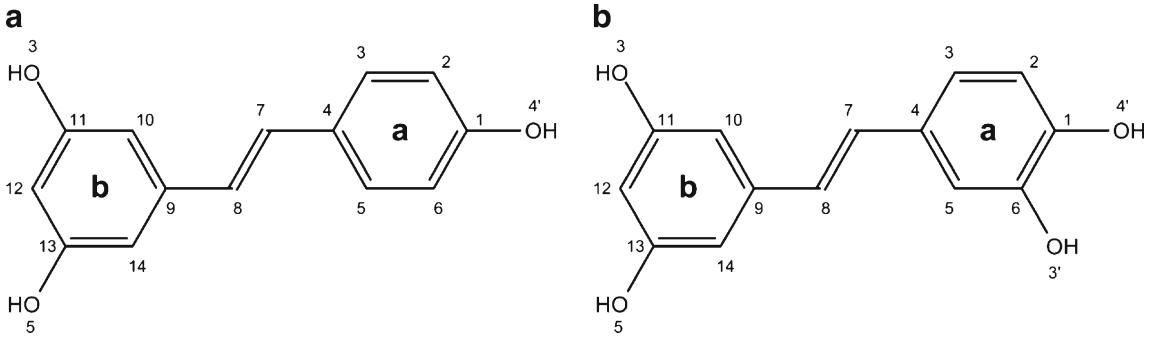

Fig. 1 Structures of *trans*-resveratrol (**a**) and *trans*-piceatannol (**b**)

was almost planar in the solid phase, with dihedral angles of 3.0° and 8.0°. Its crystal structure revealed the richness of the dynamics its hydrogen bonds. The distances associated with these intermolecular interactions for some oxygen atoms indicates high disorder in the crystal form. Moreover, the three-dimensional solid-state structure of *t*-RES shows flip-flop motions of three hydroxyl groups. Numerous spectroscopic experiments on *t*-RES have been performed, providing infrared [4], resonance Raman [5], and low-temperature fluorescence [6] spectra.

In parallel with such experimental studies, theoretical calculations of the molecular structure of *t*-RES have also been performed. Caruso et al. [3] presented results obtained with density functional theory (DFT) and compared them with experimental data. They optimized the geometry of *t*-RES in the gas state by energy minimization. A similar procedure was also applied to the anions. The authors used the Perdew–Wang (PWC) [7] functional and double numerical basis sets with polarization functions (DNP) [8] for all atoms in the molecule studied. Based on the optimized structure, they determined the rotational (energy) barrier for the phenyl rings containing hydroxyl groups. It was also shown that its maximum single-point energy is 7.3 kcal mol^{-1} higher than that of the totally planar structure. This observation indicates that the ground-state conformation of *t*-RES in a vacuum is practically planar, and that there is a good correlation between theoretical results and the X-ray diffraction data.

An attempt to determine the molecular structure of *trans*-resveratrol was also undertaken by Bernard et al. [9]. In their work, the structure of *trans*-resveratrol was studied using Hartree–Fock (HF) and DFT calculations. For the molecule analyzed, the geometry obtained at the B3LYP/6-31 G(d,p) level was strictly planar. Furthermore, an investigation performed at the HF/6-31 G(d,p) level predicted that the dihedral angles α and θ of this molecule are approximately 24°. This value is in agreement with the value of 23° obtained previously with the 6-31 G(d) basis set. Also, Andreev et al. [10] obtained 46.6° for the dihedral angles α and θ by applying a restricted HF method.

Trans-piceatannol (Fig.1b) is found in grapes [11], peanuts [12], berries [13] and various species with *t*-RES [14]. In human cells, *t*-PIC is the main product of the metabolism of *t*-RES, which involves cytochrome P450 enzymes [15, 16]. This compound shows antioxidant [17], antimicrobial [18], and anti-inflammatory [19] activities. Recently, the molecular structure of *t*-PIC was solved by Rossi et al. [20] using X-ray diffraction. Their studies demonstrated that *t*-PIC is characterized by a strictly planar geometry. Very strong intermolecular hydrogen bonds in its crystal structure were noted. Moreover, these authors claimed that the strong antioxidant activity of this polyphenol is due to hydrogen-bond formation. As well as obtaining experimental data, Rossi et al. performed a theoretical investigation of the structural features of *t*-PIC using DFT and the COSMO solvation model [21] for the effect of water solvent. This demonstrated that *t*-PIC has a planar geometry, and is a more efficient scavenger of hydroxyl and peroxyl radicals than *t*-RES [20].

All of the abovementioned experimental data and promising potential applications of these two compounds motivated us to investigate them theoretically, using MP2 perturbation theory for geometry analysis. Our work represents the first time that this method has been used to perform an ab initio investigation of the molecular structures of these two polyphenols. Note that MP2 is a correlation method, and MP2 geometries are usually quite accurate. Furthermore, for the chemical species investigated, accurately accounting for the electron correlation is crucial to accurately predicting their geometrical features. One of the objectives of the work described in the present paper was to investigate the nature of the stacking interaction between two TR molecules mainly from the viewpoint of the dispersion, induction, and electrostatic forces. Another aim of this work was to compare the results obtained using the quantum description of the stacking interaction with those obtained using the B3LYP functional, the Hartree–Fock method, and MP2 perturbation theory. Quantum calculations were applied to study the vertical separation and twist angle dependence of the stacking energy and to identify the most energetically stable conformer of the *t*-RES dimer on the potential energy surface (PES).

Quantum-chemical computations

All calculations reported in this work were performed within the GAUSSIAN 03 computational package [22]. Structural and total molecular energy optimizations were carried out in vacuum without symmetry constraints in the ground state. For each structure, the force constants at the initial point of optimization were computed using the same methods and basis sets as used for the optimization procedure. Initially, the structures of *t*-RES and *t*-PIC were fully optimized using

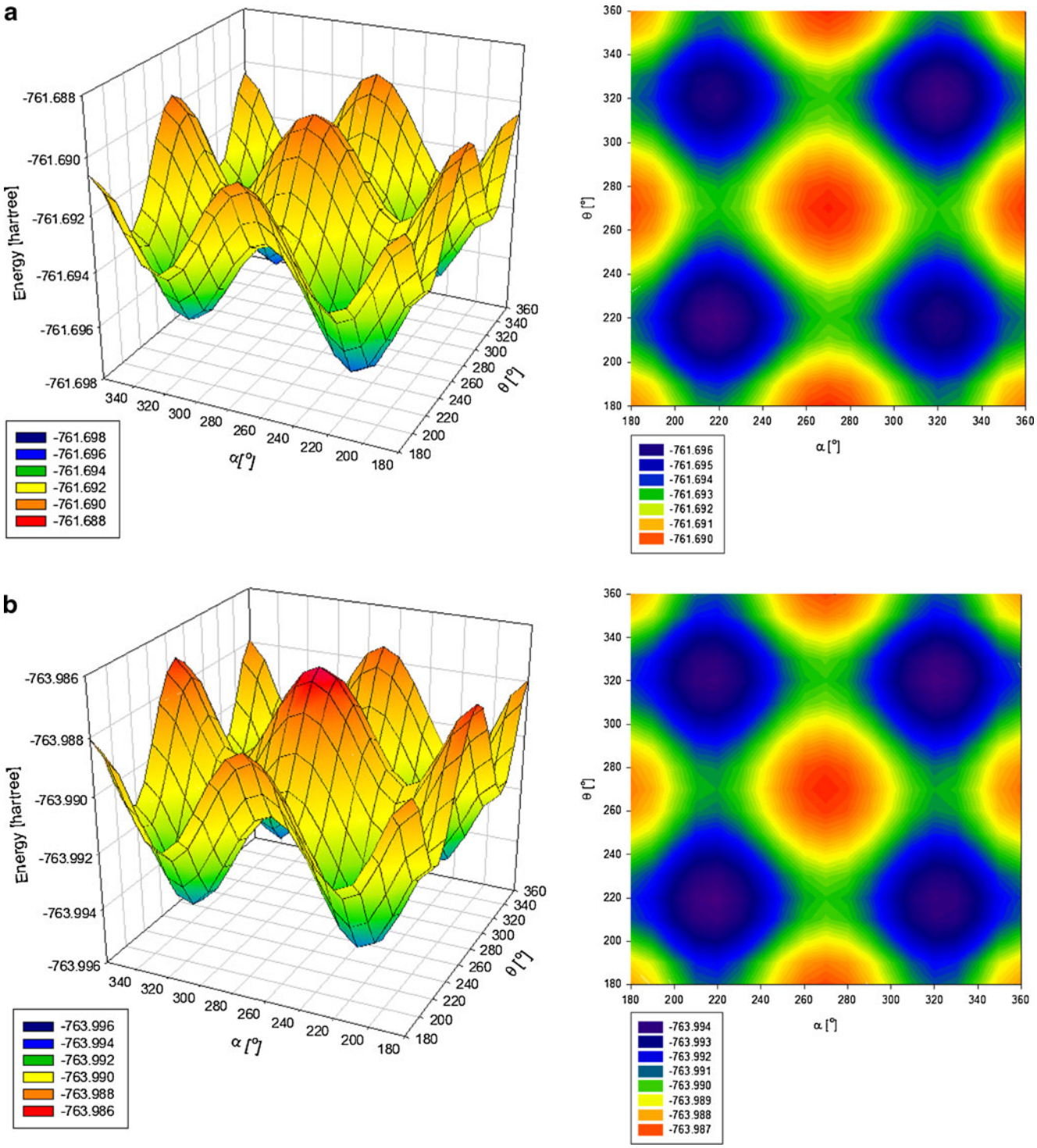

Fig. 2 HF/6-31G(d) (**a**) and MP2(full)/6-31G(d) (**b**) conformational energy maps and 3-D PESs (based on α and θ coordinates) for *trans*-resveratrol in vacuum

a restricted Hartree–Fock (HF) method combined with the 6-311+G(d,p) basis set. In the next step, the most stable HF geometries of *t*-PIC and *t*-RES were fully optimized at the restricted MP2(full)/6-31 G(d), MP2(full)/6-31+G(d), MP2 (full)/6-31 G(d,p), MP2(full)/6-31+G(d,p), MP2(full)/6-311 G(d,p), MP2(full)/6-311 G(d,p), MP2(full)/6-311+G(d,p), MP2(full)/6-311++G(d,p), and MP2(full)/aug-cc-pVTZ levels. To confirm the positions of the minima, HF geometry optimization was performed, starting from the most stable conformations obtained from a scan of the PES with partial optimization. Potential energy surfaces (Fig. 2) were built by varying the dihedral angles α (C_5–C_4–C_7–C_8) and θ (C_7–C_8–C_9–C_{10}) in the compounds studied. The conformational energy maps were obtained through discrete rotation of these selected dihedral angles in 10° increments from 0° to 180°. At each point, the total energy of *t*-RES was computed at the HF/6-31 G(d) and MP2(full)/6-31 G(d) levels of theory (Fig. 2), while the total energy of *t*-PIC was computed at the B3LYP/6-31 G(d) and HF/6-31 G(d) levels. Afterwards, the most stable structures obtained from the energy profiles were fully optimized without any geometrical and symmetry constraints around each potential minimum.

Since the relative orientations of the hydrogens in OH groups comprise another very important geometrical parameter, potential energy surfaces describing the relation between these orientations and the total energy were built for the most stable geometries obtained from the full optimizations. These surfaces were generated at the restricted HF/6-31 G(d) and MP2(full)/6-31 G(d) levels by varying the dihedral angles β (C_6–C_1–$O_{4'}$–$H_{4'}$), γ (C_{10}–C_{11}–O_3–H_3), φ (C_{14}–C_{13}–O_5–H_5), and δ (C_{11}–C_{12}–$O_{4'}$–$H_{4'}$) in 60° increments, constraining all other geometrical parameters. In the calculations, we varied the angle by 60° in order to find out whether the hydrogen atoms in the OH groups in the most stable conformations are oriented in the plane of the molecule or out of the plane.

Finally, for each fully optimized structure, frequency analysis at the same level of theory was used to verify whether the structure corresponded to a stationary point on the potential energy surface. In this way, the structures of *t*-RES and *t*-PIC corresponding to absolute energy minima were determined. Harmonic vibrational frequencies for all optimized structures were calculated analytically, checking that the eigenvalues of the Hessian matrix were positive; that is, that the geometries were true energetic minima. The harmonic vibrational frequencies and zero-point energy corrections were scaled by a factor of 0.973.

Full optimization of the geometry of the *t*-RES dimer was performed at the B3LYP/6-311+G(d,p) level of theory. Finally, to more accurately predict the total energies of the fully optimized geometries of these dimeric conformers, single point energy calculations were performed at the MP2(full)/6-311 G(d,p), MP2(full)/6-311+G(d,p), MP2 (full)/6-311++G(d,p), MP2(full)/aug-cc-pVDZ, MP2(full)/aug-cc-pVTZ, and MP2(full)/aug-cc-pVQZ levels. The relative stabilities of the dimeric conformers were evaluated via these single point energies. Employing the MP2 theory (with the frozen core approximation), we evaluated the influence of electron correlation effects on the stabilization energies. All MP2 calculations were performed with all electrons active. The stabilization energies ΔE_{stab} of *t*-RES dimers were computed in a supermolecular approach using the following formula reported by Pavelka et al. [23]:

$$\Delta E_{\text{stab}} = -\left(E_{\text{dimer}} - \sum_{i}^{\text{monomers}} E(i)\right), \tag{1}$$

where E_{monomer} is the total energy of the fully optimized geometry of an individual subsystem (*t*-RES). The intermolecular energies of the conformers studied were computed as the sum of the Hartree–Fock and Coulomb electron correlation contributions. The full function counterpoise method developed by Boys and Bernard [24] was employed for both energy components to eliminate the basis set superposition error (BSSE). The stabilization energies of the selected dimeric conformers were determined at the MP2(full)/6-311 G(d,p), MP2(full)/6-311+G(d,p), MP2(full)/6-311++G (d,p), MP2(full)/aug-cc-pVDZ, MP2(full)/aug-cc-pVTZ,

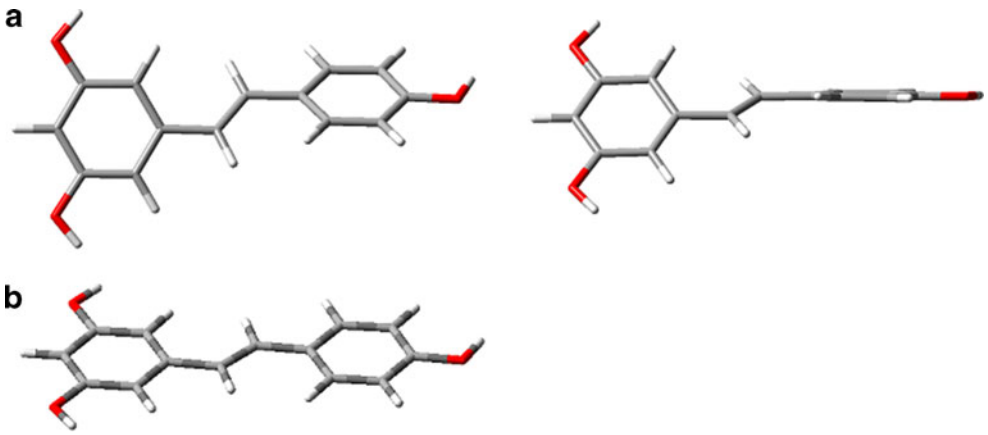

Fig. 3 The fully optimized structure of *trans*-resveratrol calculated at the MP2(full)/6-311G(d,p) (**a**) and MP2(full)/aug-cc-pVTZ (**b**) levels

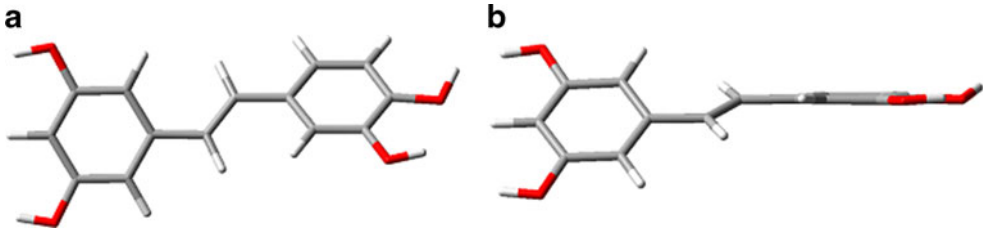

Fig. 4 The fully optimized structure of *trans*-piceatannol calculated at the MP2(full)/6-311G(d,p) level

MP2(full)/aug-cc-pVQZ, and B3LYP/6-311 G(d,p) levels. It is well known that hydration effects can have a considerable influence on the formation of the *t*-RES dimer. Considering the complexity of these computations, hydration effects and the polarized continuum solvation model will be investigated in detail in future studies.

Results and discussion

Geometry analysis of *t*-RES and *t*-PIC

Geometrical parameters of the fully optimized structures of *t*-RES (Fig. 3) calculated in vacuum at the MP2(full)/6-311 G(d,p) and MP2(full)/aug-cc-pVTZ levels, and those of *t*-PIC at the MP2/6-311 G(d,p) level (Fig. 4), are displayed in Tables 1 and 2. Optimization of the structures of *t*-RES and *t*-PIC leads to the true energy minima on the potential energy surfaces, as confirmed by the lack of imaginary frequencies. The bond lengths obtained are consistent with experimental values, while the calculated angles disagree with the experimental data [3, 18]. Some are reasonable while others have errors of several degrees. If we consider the results obtained using the 6-31 G(d), 6-31+G(d), 6-31 G(d,p), 6-31+G(d,p), 6-311 G(d,p), 6-311+G(d,p), and 6-311++G (d,p) basis sets, it is clear that the dihedral angles α and θ have large values. Hence, the geometries of *t*-RES and *t*-PIC deviate strongly from planarity. This result does not correlate with DFT calculations performed previously [25–27]. The MP2 finding obtained for *t*-RES in this study is in good agreement with previous HF computations.

However, using the correlation-consistent polarized valence triple zeta basis set proposed by Dunning (aug-cc-pVTZ), the dihedral angles α and θ of *t*-RES and *t*-PIC are practically zero (Table 2). Thus, the result obtained at the advanced MP2(full)/aug-cc-pVTZ level proves that, using a very large correlation-consistent basis set, the geometries of *t*-RES and *t*-PIC are planar. This result is in excellent agreement with B3LYP computations performed with the 6-31 G (d), 6-31+G(d), 6-31 G(d,p), 6-31+G(d,p), 6-311 G(d,p), 6-311+G(d,p), 6-311++G(d,p), and aug-cc-pVTZ basis sets. The DFT computations performed using this spectrum of basis sets demonstrate that the equilibrium electronic geometry of *t*-PIC is also strictly planar. Taking into account the fact that a planar structure is highly preferable in biological systems (planar compounds are effective intercalators and antioxidants), we can conclude that the results obtained at

Table 1 The optimized bond lengths (in Å) of *trans*-resveratrol and *trans*-piceatannol, as calculated by the MP2 method

Bond	*Trans*-resveratrol		*Trans*-piceatannol
	MP2/6-311G (d,p)	MP2/aug-cc-pVTZ	MP2/6-311G (d,p)
O(4′)–C(1)	1.366	1.380	1.377
O(3′)–C(6)	—	—	1.361
O(3)–C(11)	1.368	1.382	1.369
O(5)–C(13)	1.367	1.382	1.368
O(4′)–H(4′)	0.962	0.968	0.961
O(3′)–H(3′)	—	—	0.965
O(3)–H(3)	0.962	0.968	0.961
O(5)–H(5)	0.962	0.968	0.961
C(1)–C(2)	1.400	1.406	1.393
C(2)–C(3)	1.396	1.405	1.398
C(4)–C(7)	1.466	1.469	1.465
C(7)–C(8)	1.354	1.364	1.354
C(8)–C(9)	1.467	1.471	1.468
C(10)–C(11)	1.398	1.404	1.395
C(12)–C(13)	1.396	1.403	1.399

Table 2 The optimized angles (in degrees) of *trans*-resveratrol and *trans*-piceatannol, as calculated by the MP2 method

Angle	*Trans*-resveratrol		*Trans*-piceatannol
	MP2/6-311G (d,p)	MP2/aug-cc-pVTZ	MP2/6-311G(d,p)
C(5)–C(4)–C(7)–C(8)	25.5	0.7	22.4
C(7)–C(8)–C(9)–C(10)	28.2	0.8	25.7
C(2)–C(1)–O(4')–H(4')	0.3	0.3	17.8
C(1)–C(6)–O(3')–H(3')	—	—	3.3
C(10)–C(11)–O(3)–H(3)	1.8	0.7	176.0
C(14)–C(13)–O(5)–H(5)	0.0	0.3	179.5
O(4')–C(1)–C(2)	123.2	123.1	124.8
O(4')–C(1)–C(6)	117.3	116.9	114.9
O(3)–C(11)–C(10)	122.5	122.5	117.2
O(3)–C(11)–C(12)	116.7	116.2	122.1
O(5)–C(13)–C(12)	116.8	116.5	122.3
O(5)–C(13)–C(14)	122.6	122.572	117.3
Energy (hartrees)	−764.39630851	−764.94262842	−839.47320043

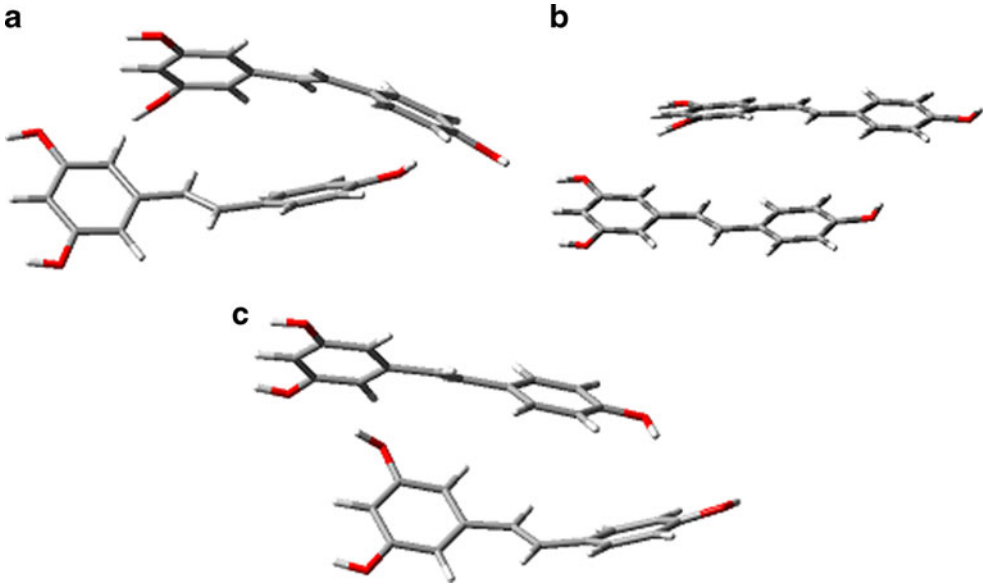

Fig. 5 B3LYP/6-311+G(d,p) optimized geometries of the parallel-displaced conformers of the *t*-RES dimer

the MP2(full)/aug-cc-pVTZ and B3LYP/aug-cc-pVTZ levels are reflected in the biomedicinal activities of *t*-RES and *t*-PIC.

It should be emphasized that Kwasniewski et al. [28] have proven that *trans*-stilbene is a strictly planar molecule in its absolute minimum energy form. This result has been confirmed by MP2 and DFT optimization through the use of the aug-cc-pVDZ basis set [28]. However, in our study, we found that the geometry of *t*-RES is planar at the MP2(full)/aug-cc-pVTZ and B3LYP/aug-cc-pVTZ levels.

It should be emphasized that this result obtained at the MP2(full)/6-311 G(d,p) level (Table 2) does not agree with the experimental data obtained by Caruso et al. [3], who, on the basis of X-ray diffraction spectra, claimed that *t*-RES deviates slightly from planarity in the solid phase at room temperature. In our opinion, the crystalline and isolated structures of each molecule investigated can differ substantially from each other because their molecular environments are different.

In both of the compounds studied, the optimal values of the O–H and C–C bond lengths are similar (Table 1). The optimized values of the dihedral angles C2–C1–O4′–H4′ and C10–C11–O3–H3 in *t*-PIC (Table 2) prove that the hydrogen atoms of the O4′H4′ and O3H3 groups do not

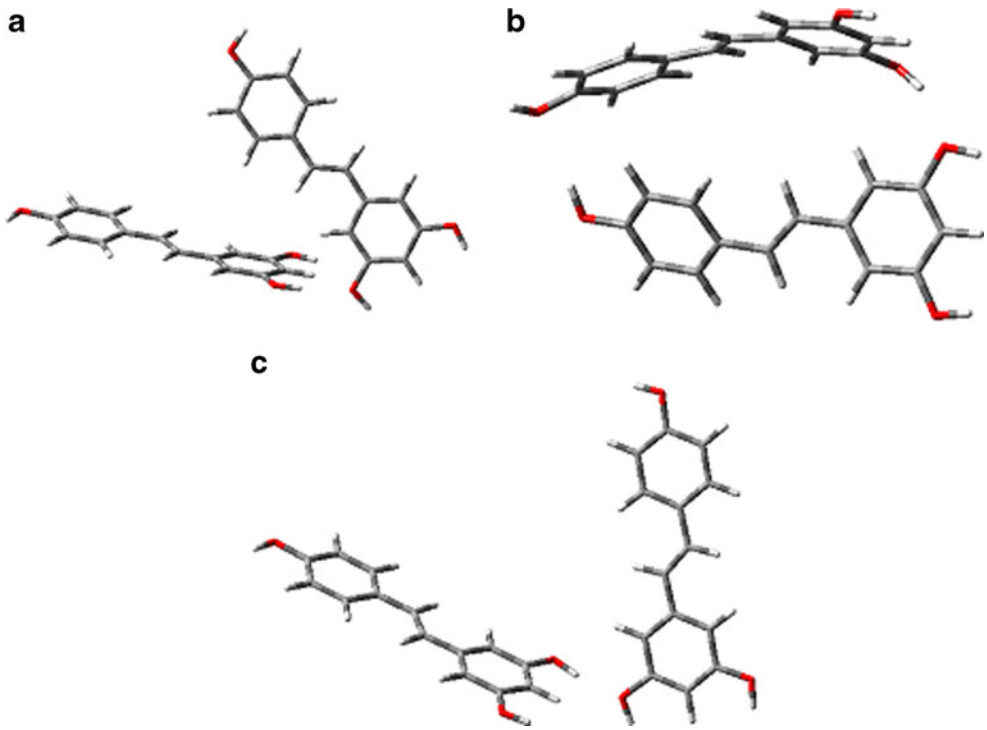

Fig. 6 B3LYP/6-311+G(d,p) optimized geometries of the T-stacked conformers of the *t*-RES dimer

lie in the plane of the phenyl rings. However, according to the optimized values of these dihedral angles in *t*-RES, we can conclude that the H atoms of all OH groups lie in the plane of the phenyl rings. The energy barrier to the rotation of the hydrogen atom of the OH group in *t*-RES computed at the MP2(full)/6-311 G(d,p) level is 1.2 kcal mol^{-1}. Hence, this atom is very labile at room temperature. Based on the conformational MP2(full)/6-31 G(d) (Fig. 2b) profile, we calculated the relative energies of the planar conformations of *t*-RES versus their nonplanar minima. For each stationary point on the PES, single point energy calculations were carried out using the MP2(full)/aug-cc-pVTZ method. The results obtained indicate that the most significant value of this energy is 1.88 kcal mol^{-1}. This barrier is smaller than the value of kT at 298.15 K, and so the geometry of *t*-RES is very susceptible to rotation about the single C–C bond linked to the vinyl bond.

The stacking interaction between *t*-RES molecules

Conformational analysis (B3LYP/6-311+G(d,p)) of *t*-RES dimers reveals 30 stable stacked conformers at the true energy minima on the potential energy surface (PES). However, only six conformers have considerable relative energies, so those conformers were analyzed. Some of the energy-minimized structures were discarded because they corresponded to saddle points or because their energies were >10 kJ mol^{-1} above the average energy of the local minima. Three parallel-displaced and three T-stacked conformers were identified with regard to nonbonded interactions between the aromatic rings. To obtain more reliable intermolecular energies, in the next step, MP2 single point energy calculations were employed for these six minimized geometries. It should be stressed that the B3LYP/6-311+G(d,p) method satisfactorily reproduced the geometries of the parallel-displaced (Fig. 5a–c) and T-shaped conformers (Fig. 6a–c). The relative energies of the *t*-RES dimeric conformers obtained at various levels of theory are given in Table 3. The relative MP2 single point calculations demonstrated that conformer **6a** is the most energetically stable,

Table 3 Computed relative energies (kcal mol^{-1}) of the energetically stable dimeric conformers

Quantum method	7a	7b	7c	8a	8b	8c
B3LYP/6-311g(d,p)	4.66	4.03	4.58	7.51	5.43	7.40
MP2/6-311g(d,p)	4.73	4.16	4.71	7.68	5.55	7.53
MP2/6-311+g(d,p)	4.21	3.82	4.32	7.04	5.21	7.20
MP2/6-311++g(d,p)	4.13	3.69	4.14	6.85	5.02	7.07
MP2/aug-cc-pVDZ	6.79	5.34	6.47	8.35	6.83	7.87
MP2/aug-cc-pVTZ	6.91	5.55	6.85	8.98	7.04	7.98
MP2/aug-cc-pVQZ	7.24	6.51	7.17	9.56	7.36	8.22

Table 4 Computed stabilization energies including the BSSE contribution (kcal mol^{-1}) of the energetically stable dimeric conformers

Quantum method	7a	7b	7c	8a	8b	8c
B3LYP/6-311g(d,p)	2.85	3.49	2.93	0.00	2.08	0.03
MP2/6-311g(d,p)	3.33	3.79	3.37	0.00	2.26	0.26
MP2/6-311+g(d,p)	2.54	3.21	3.27	0.00	1.94	0.11
MP2/6-311++g(d,p)	2.26	3.03	3.12	0.00	1.81	0.09
MP2/aug-cc-pVDZ	4.68	4.97	4.24	0.00	3.89	1.87
MP2/aug-cc-pVTZ	4.81	5.21	4.32	0.00	3.92	1.98
MP2/aug-cc-pVQZ	5.12	5.38	4.87	0.00	4.15	2.12

and this has a T-stacking (edge-to-phase) geometry. It should be stressed that the distorted T-shaped structure is among the most stable structures of benzene dimers [29]. The MP2 stabilization energies (Table 4) show the same trend in dimeric conformer stability. Relatively large values of ΔE_{stab} prove that the *t*-RES molecules in these dimers are strongly bonded. It should be mentioned that the charges localized on the O(3) and O(5) atoms are slightly more negative than that on the O4′ atom (Table 5). The presence of these electronegative oxygen atoms facilitates the interaction between *t*-RES molecules via O...HO hydrogen bonding. In the *t*-RES dimer (see Fig. 7), the charge on the O(54) atom is lower than it is in the monomer. This is probably the result of the hydrogen-bonding interaction between the two *t*-RES stacked molecules. Due to the fact that the O...HO electronic interaction is the result of donation from the lone pair of the oxygen atom into the empty $\sigma(O–H)^*$ orbital, NBO (natural bond orbital) analysis is needed to estimate the occupation number of $\sigma(O–H)^*$.

It should be pointed out that in dimer **6a**, the *trans*-stilbene skeletons deviate from planarity. This result is

Table 5 NBO partial atomic charges in *t*-RES computed at the B3LYP/6-311+G(d,p) level

Atom	Charge
O4’	−0.358
O3	−0.361
O5	−0.363
C1	0.156
C2	−0.122
C4	−0.075
C7	−0.061
C8	−0.085
C9	−0.052
C10	−0.071
C11	0.152
C12	−0.151
C13	0.156
C14	−0.088
C3	−0.075

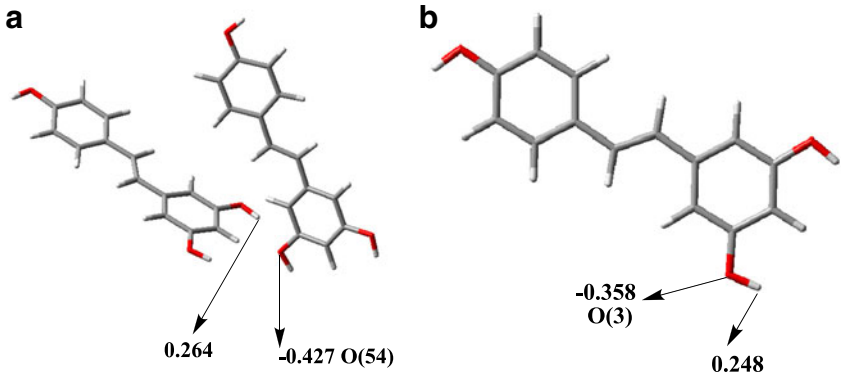

Fig. 7 Partial charges computed for the *t*-RES dimer (**a**) and monomer (**b**), computed at the B3LYP/6-311+G(d,p) level

confirmed by the optimized values of the dihedral angles: α (C_5–C_4–C_7–C_8)=3.97° and θ (C_7–C_8–C_9–C_{10})=8.95°. Moreover, this dimer includes favorable C–H...π (3.88 Å, 3.33 Å) interactions and a strong hydrogen bond (1.90 Å) between the H(27) atom of the *t*-RES molecule and the O (54) atom of the second interacting molecule (Fig. 8). From this result, we can see that these interactions provide the greatest contribution to the stability of this conformer. C–H…π interactions are observed between the H(35) and H (43) atoms in ring A of one *t*-RES molecule and the aromatic ring B of the other molecule (Fig. 8). The distances 3.88 Å and 3.33 Å are in accord with typical T-stacked geometries reported in the literature [30, 31]. To provide unambiguous evidence that a C–H…π interaction occurs in the most energetically stable T-shaped geometry, we will calculate ^{1}H NMR shifts and the *J*(C–H) coupling constant in our next study. In the conformer **6a**, the H(35) and H(43) atoms tend to be oriented perpendicular to the aromatic ring of the second molecule (Fig. 8). This observation indicates that a T-stacking interaction can occur in the *t*-RES dimer.

Dependence of the *t*-RES–*t*-RES stacking interaction energy on the vertical separation of the molecules

Recently, Caruso et al. [3] studied the X-ray structure of *t*-RES. Their results indicated that the crystal structure of *t*-RES exhibits a packing effect. The stacking distance between the molecules studied was close to 4.1 Å. Based on their experimental data, we studied the dependence of the stacking energy on the vertical distance between the interacting planar *t*-RES molecules. The stacked geometries of *t*-RES were prepared in the following way. Two *t*-RES molecules were located in the coplanar plane [sandwich

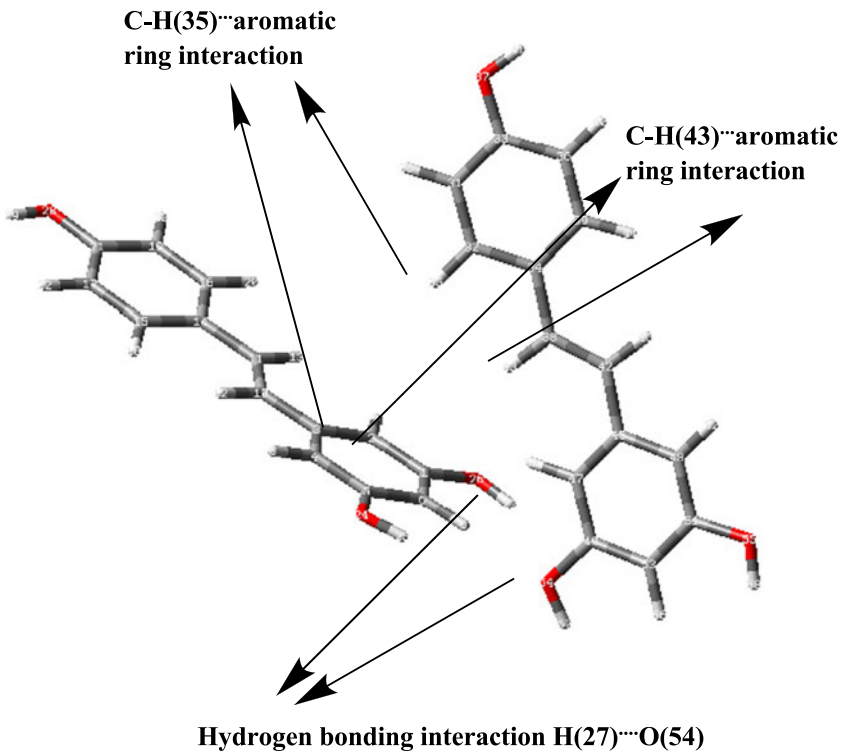

Fig. 8 The stacking and hydrogen bonding interactions in the energy minimum geometry of the T-stacked *t*-RES dimer

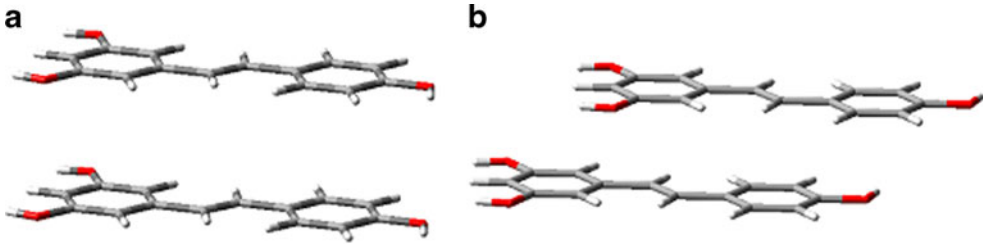

Fig. 9 Stacked models used to study the dependence of the stacking interaction energy on the vertical separation of the *t*-RES units: **a** sandwich configuration (S structure), **b** parallel-displaced configuration (PD structure)

(S) structure and parallel-displaced (PD) structure] in such a way that the axes of the main system were parallel. Then, the intersystem separation (vertical) was optimized at the MP2(full)/aug-cc-pVTZ level. The value of ΔE_{stab} for each optimized distance was determined at the MP2(full)/aug-cc-pVTZ, B3LYP/aug-cc-pVTZ, and HF/aug-cc-pVTZ levels. The use of the highly computationally intensive MP2(full)/aug-cc-pVTZ method was dictated by the need to correctly estimate the correlation energy contribution, which can be large for S-stacked conformers. The stacked models are presented in Fig. 9, while Figs. 10 and 11 provide stacking energy curves obtained by varying the separation between the *t*-RES molecules. From the results obtained, it is evident that the minimum of the MP2 curve occurs at around 4 Å, which is in excellent agreement with the distance in the crystal [3]. The MP2 curves properly describe the interaction energy in the long-range attraction region and repulsive effects at short distances. The dominant long-range forces are expected to be London dispersion forces. In further work, the decomposition of the total interaction energy into physically defined energy components will be performed using the symmetry adapted perturbation treatment (SAPT) [32]. Moreover, we will estimate the electrostatic, exchange, repulsion, charge transfer, and dispersion contributions to the total interaction energy using the energy decomposition analysis (EDA) recently developed by Su and Li [33].

However, the B3LYP and HF curves are completely different from the MP2 data. It should be stressed that these curves do not have an energy minimum. This result proves that DFT and HF methods do not include a London dispersion term. We can see that the repulsive term predominantly appears in the HF and B3LYP methods. In a subsequent study, we will use the DFTB-D method, which is a combination of the approximate tight-binding DFTB with the empirical dispersion energy. Recent computational studies have shown that this method, when extended to include a London dispersion energy term, yields satisfactory stacking energies. Moreover, we will use recently developed XC (exchange correlation) functionals to obtain a more reliable description of the stacking interaction. These functionals allow long-range dispersion effects to be properly estimated. Additionally, for the *t*-RES stacked model, we will test a dispersion-corrected MP2 method recently developed by Tkatchenko et al. [34]. This inexpensive dispersion correction scheme brings MP2 binding energies into remarkable alignment with CCSD(T) reference data.

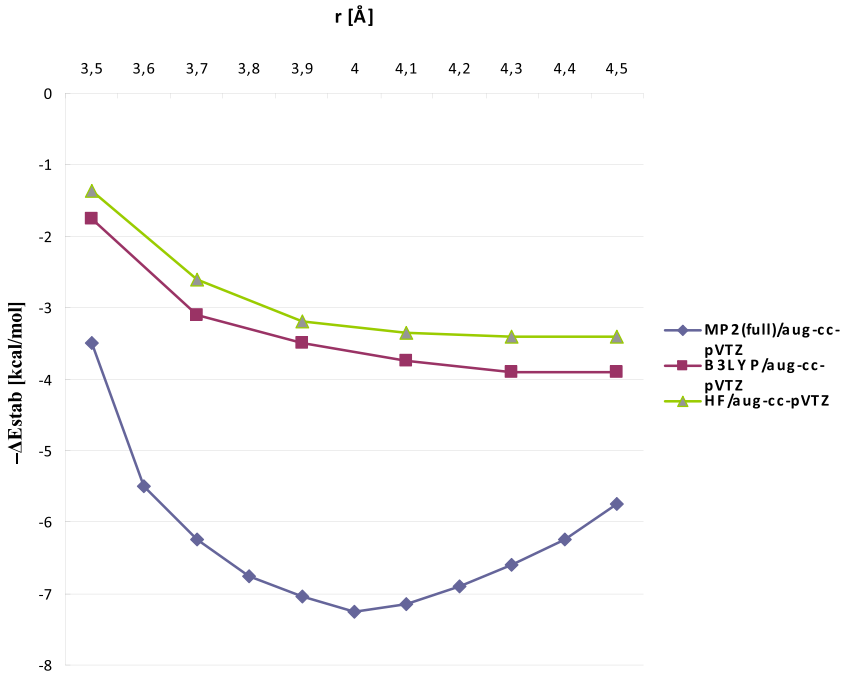

Fig. 10 Potential energy curves for the sandwich configuration of the *t*-RES dimer

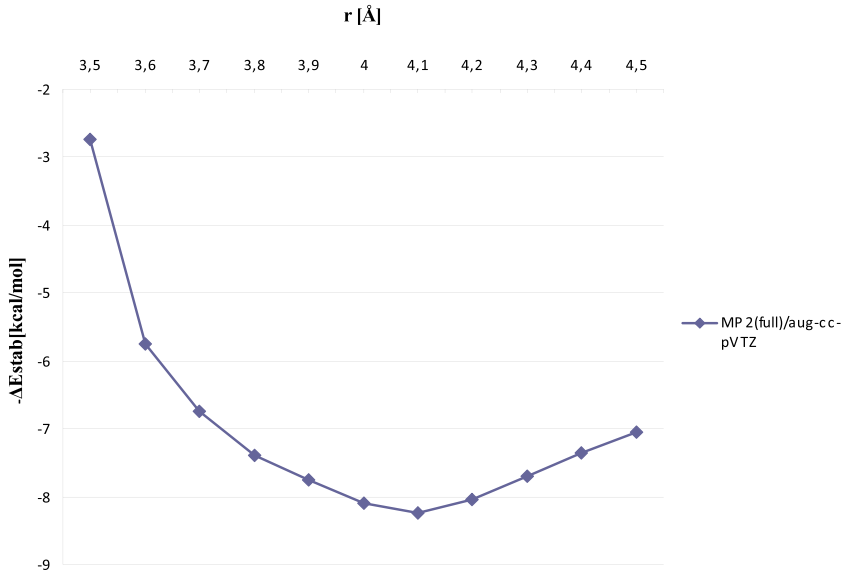

Fig. 11 Potential energy curve for the parallel-displaced configuration of the *t*-RES dimer

Twist angle dependence of the stacking energy

It is known that the stacked molecules can adopt different orientations with respect to one another. Hence, we investigated the twist dependence of the *t*-RES–*t*-RES stacking interaction via the MP2(full)/aug-cc-pVTZ method. The vertical separation of two interacting *t*-RES molecules was assumed to be 4.1 Å, and these molecules were localized in the coplanar plane (the sandwich configuration). We then twisted this initial system along the *t*-RES–*t*-RES axis in a right-handed manner. For each twisted angle, this axis passes through the center of mass of the interacting molecules. The stacking energy was computed for the whole range $\varphi \in (0; 360°)$. Figure 12 presents the MP2 values of the stacking energy (stabilization energies) for increments of 60° in the twist angle. From this curve, we can see that this energy is greatly dependent on the twist angle, and there are three energy minima. We can conclude that, for this system, the dispersion attraction depends on the overlap of the stacked system, and the dispersion is the greatest contributor to the twist-dependent stacking energy. In particular, when the stacked *t*-RES molecules overlap fully, the dispersion contribution can be significant. Moreover, it interesting to note that for a parallel orientation of the *t*-RES molecules, the dispersion term appears to be dominant. The attractive induction term is also non-negligible, and depends strongly on the overlap of the *t*-RES molecules.

Conclusions

In order to determine reliable structures for *trans*-resveratrol and *trans*-piceatannol in a vacuum, accurate quantum chemical calculations were performed utilizing MP2 and DFT methods. The geometric properties of isolated *t*-RES molecules and the stacking interaction between them were examined. The geometry optimization procedure was carried out with the aid of a wide spectrum of basis sets. The results

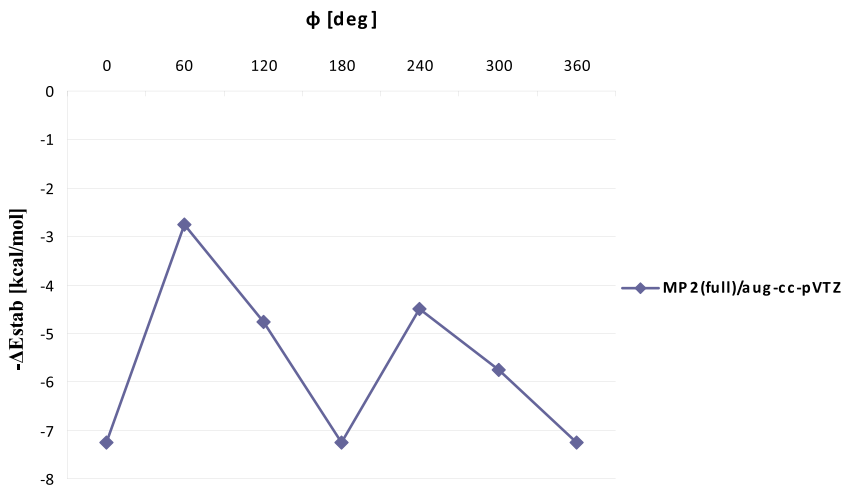

Fig. 12 Potential energy curve for the twist angle dependence of the stabilization energy of the *t*-RES dimer

obtained indicate that *trans*-resveratrol and *trans*-piceatannol have planar geometries at the MP2(full)/aug-cc-pVTZ and B3LYP/aug-cc-pVTZ levels. MP2 potential energy curves demonstrated that the London dispersion contribution to the stacking energy cannot be neglected. Further computations are needed to determine the quantitative contributions of the London energy to the total stabilization energies of the dimeric systems studied. However, the B3LYP exchange-correlation functional and the HF method completely failed to localize any energy minimum on the potential energy curve. Thus, the use of the B3LYP functional and the HF method to study the stacking interaction between planar polyphenolic derivatives of *trans*-stilbene is not recommended. It was found that the most stable dimer of *t*-RES is characterized by T-stacking interactions, and is mainly stabilized by hydrogen bonding and favorable C–H…π interactions. Our computations predict that, except for amino acids in proteins [35, 36] and carbon aromatic cycles (benzene and naphthalene), stilbenoids are able to form T-shaped structures. Energetically stable parallel-displaced conformers were found on the potential energy surface. The computed value of the stacking distance between strictly planar *t*-RES molecules is in excellent agreement with X-ray data. It has been shown that the dispersion energy contribution plays a crucial role in the twist-dependent stacking process. Summarizing, the results presented here prove that there is a π–π stacking interaction between *t*-RES molecules. This observation has been experimentally confirmed by Bonechi et al. [37]. We hope that the stacking interactions studied here will help to explain the numerous biological properties of *t*-RES.

Acknowledgments This study is supported by a grant from the Supercomputer Centre in Poznań: "Investigation of the biophyschemical properties of *trans*-resveratrol." We are indebted to Professor Jerzy Konarski and Dariusz Lasecki for many helpful and stimulating discussions, as well as to M.Sc. Maria Spychalska for linguistic assistance.

References

1. Frémont L (2000) Biological effects of resveratrol. Life Sci 66:663–673
2. Sanders TH, McMichael RW, Hendrix KW (2000) Occurrence of resveratrol in edible peanuts. J Agric Food Chem 48:1243–1246
3. Caruso F, Tanski J, Villagas-Estada A, Rossi M (2004) Structural basis for antioxidant activity of *trans*-resveratrol: ab initio calculations and crystal and molecular structure. J Agric Food Chem 52:7279–7285
4. Edelmann A, Diewok J, Schuster KC, Lendl B (2001) Rapid method for the discrimination of red wine cultivars based on mid-infrared spectroscopy of phenolic wine extracts. J Agric Food Chem 49:1139–1145
5. Scanlan JD, Bernhardson D, Smith JM (2004) In: Proc 227th ACS National Meeting on Resonance Raman and Computational Study of Resveratrol and Related Derivatives, Anaheim, CA, USA, 28 Mar–1 Apr 2004
6. Lin CH, Chen YH (2001) On-line identification of *trans*- and *cis*-resvertarol nonaqueous capillary by electrophoresis/fluorescence spectroscopy at 77 K. Electrophoresis 22:2574–2579
7. Perdew JP, Wang Y (1992) Accurate and simple analytic representation of the electron gas correlation energy. Phys Rev B 45:13244–13249
8. Delley B (1996) Fast calculations of electrostatics in crystals and large molecules. J Phys Chem 100:6107–6110
9. Bernard E, Britz-McKibbin P (2007) Resveratrol photoisomerization: an integrative guided-inquiry experiment. J Chem Educ 84:1159–1161
10. Andreev GN, Korte EH, Jordanov BN, Schrader B (1997) Polarized FT Raman spectra of *trans*-stilbene oriented in the nematic liquid crystal host 4-alkyl-4′-cyanobicyclohexyl. J Mol Struct 408:305–308
11. Bavaresco L, Fregoni M, Trevisan M, Mattivi F, Vrhovsek U, Falchetti R (2002) The occurrence of piceatannol in grape. Vitis 41:133–136
12. Ku KL, Chang PS, Cheng YC, Lien CY (2005) Production of stilbenoids from the callus from *Arachis hypogaea*: a novel source of the anticancer compound picetannol. Agric Food Chem 53:3877–3881
13. Rimando AM, Kalt W, Magee JB, Dewey J, Ballington JR (2004) Resveratrol, pterostilbene and piceatannol in *Vaccinium* berries. J Agric Food Chem 52:4713–4719
14. Lin L, Lien C, Cheng Y, Ku K (2007) An effective sample preparation approach for screening the anticancer compound piceatannol using HPLC coupled with UV and fluorescence detection. Anal Technol Biomed Life Sci 853:175–179
15. Potter GA, Patterson LH, Wanogho E, Perry PJ, Butler PC, Ijaz T, Ruparelia KC, Lamb JH, Farmer PB, Stanley LA, Burke MD (2002) The cancer preventative agent resveratrol is converted to the anticancer agent piceatannol by the cytochrome P450 enzyme CYP1B1. Br J Cancer 86:774–778
16. Piver B, Fer MX Vitrac X, Merillon J, Dreano Y, Berthou F, Lucas D (2004) Involvement of cytochrome P450 1A2 in the biotransformation of *trans*-resveratrol in human liver microsomes. Biochem Pharmacol 68:773–778
17. Wung BS, Hsu MC, Wu CC, Hsieh CW (2006) Piceatannol upregulates endothelial heme oxygenase-1 expression via novel protein kinase C and tyrosine kinase pathways. Pharmacol Res 53:113–122
18. Richard N, Porath D, Radspieler A, Schwager J (2005) Effects of resveratrol, piceatannol, tri-acetoxystilbene, and genistein on the inflammatory response of human peripheral blood leukocytes. J Mol Nutr Food Res 49:431–442
19. Docherty JJ, McEwen HA, Sweet TJ, Bailey E, Booth TD (2007) Resveratrol inhibition of *Propionibacterium acnes*. J Antimicrob Chemother 59:1182–1184
20. Rossi M, Caruso F, Opazo C, Salciccioli J (2008) Crystal and molecular structure of piceatannol; scavenging features of resveratrol and piceatannol on hydroxyl and peroxyl radicals and docking with transthyretin. J Agric Food Chem 56:10557–10566
21. Klamt A, Schueuermann G (1993) A new approach to dielectric screening in solvents with explicit expression for screening energy and its gradient. J Chem Soc Perkin Trans 2:799
22. Frisch MJ, Trucks GW, Schlegel HB, Scuseria GE, Roob MA, Cheeseman JR, Montgomery JA, Vreven T, Kudin KN, Burant JC, Millam JM, Iyengar SS, Tomasi J, Barone V, Menucci B, Cossi M, Scalmani G, Rega N, Petersson GA, Nakatsuji H, Hada M, Ehara M, Toyota K, Fukuda R, Hasegawa J, Ishida M, Nakajima T, Honda Y, Kitao O, Nakai H, Klene M, Li X, Knox JE, Hratchian HP, Cross JB, Bakken V, Adamo C, Jaramillo J, Gomperts R, Stratmann RE, Yazyev O, Austin AJ, Cammi R, Pomelli C, Ochterski JW, Ayala Y, Morokuma K, Voth GA, Salvador P, Dannenberg JJ,

Zakrzewski VG, Dapprich S, Daniels AD, Strain MC, Farkas O, Malick DK, Rabuck AD, Raghavachari K, Foresman JB, Ortiz JV, Cui Q, Baboul AG, Clifford S, Ciosłowski J, Stefanov BB, Liu G, Liashenko A, Piskorz P, Komaromi I, Martin RL, Fox DJ, Keith T, Al-Laham MA, Peng CY, Nanayakkara A, Challacombe M, Gill PMW, Johnson B, Chen W, Wong MW, Gonzalez C, Pople JA (2004) Gaussian 03, revision C.02. Gaussian Inc., Wallingford

23. Pavelka M, Shukla MK, Leszczyński J, Burda JV (2008) Theoretical study of hydrated copper(II) interactions with guanine:a computational density functional theory study. J Phys Chem A 112:256–267
24. Boys SF, Bernard F (1970) The calculation of small molecular interactions by the differences of separate total energies. Some procedures with reduced errors. Mol Phys 19:553–566
25. Xu S, Wang G, Liu HM, Wang LJ, Wang HF (2007) A $Dmol^3$ study on the reaction between *trans*-resveratrol and hydroperoxyl radical: dissimilarity of antioxidant activity among O-H groups of trans-resveratrol. J Mol Struct 809:79–85
26. Mikulski D, Górniak R, Molski M (2010) A theoretical study of the structure–radical scavenging activity of *trans*-resveratrol analogues and *cis*-resveratrol in gas phase and water environment. Eur J Med Chem 45:1015–1027
27. Mikulski M, Szeląg M, Molski M (2011) Quantum-chemical study of interactions of *trans*-resveratrol with guanine-thymine dinucleotide and DNA nucleobases. J Mol Model 17:3085–3102
28. Kwasniewski SP, Cleas L, François JP, Deleuze MS (2003) High level theoretical study of the structure and rotational barriers of *trans*-stilbene. J Chem Phys 118:7823–7836
29. DiStasio RA Jr, von Helden G, Steele RP, Head-Gordon M (2007) On the T-shaped structures of the benzene dimer. Chem Phys Lett 437:277–283
30. Sinnokrot MO, Sherrill CD (2004) Highly accurate coupled cluster potential energy curves for the benzene dimer: sandwich, T-shaped, and parallel-displaced configurations. J Phys Chem A 108:10200–10207
31. Sinnokrot MO, Sherrill CD (2004) Substituent effects in π–π interactions: sandwich and T-shaped configurations. J Am Chem Soc 126:7690–7697
32. Jeziorski B, Moszynski R, Szalewicz K (1994) Perturbation theory approach to intermolecular potential energy surfaces of van der Waals complexes. Chem Rev 94:1887–1930
33. Su P, Li H (2009) Energy decomposition analysis of covalent bonds and intermolecular interactions. J Chem Phys 131:014102
34. Tkatchenko A, DiStasio RA Jr, Head-Gordon M, Scheffler M (2009) Dispersion-corrected Møller–Plesset second-order perturbation theory. J Chem Phys 131:094106
35. Chakrabarti P, Bhattacharyya R (2007) Geometry of nonbonded interactions involving planar groups in proteins. Prog Biophys Mol Biol 95:83–137
36. Chelli R, Gervasio FL, Procacci P, Schettino V (2002) Stacking and T-shape competition in aromatic–aromatic amino acid interactions. J Am Chem Soc 21:6133–6143
37. Bonechi C, Martini S, Magnani A, Rossi C (2008) Stacking interaction study of *trans*-resveratrol (*trans*-3,5,4′-trihydroxystilbene) in solution by nuclear magnetic resonance and Fourier transform infrared spectroscopy. Magn Reson Chem 46:625–629